Cell Reports
Physical Science

CellPress
OPEN ACCESS

Article

# Current-driven solvent segregation in lithium-ion electrolytes

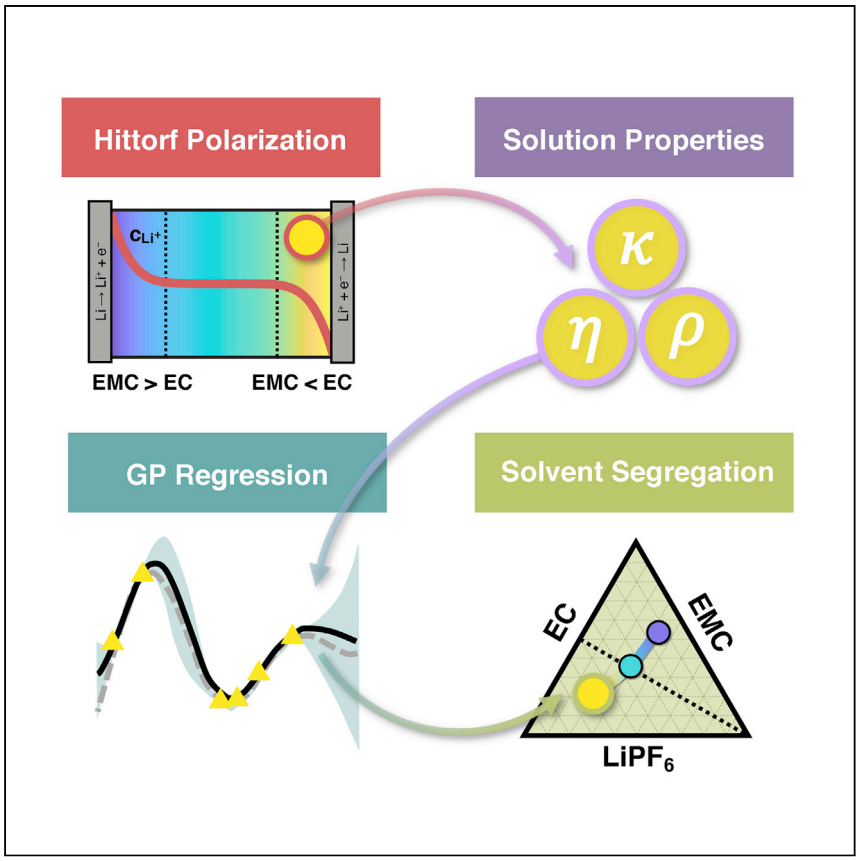


While it is understood that electrolyte solvents are consumed throughout the lifetime of battery operation, less is known about intra-cycle variation in cosolvent composition. Wang et al. pair polarization experiments with machine learning to measure solvent segregation occurring under applied current. This effect is especially prominent near electrode surfaces and may illuminate guiding principles for electrolyte design.

Andrew A. Wang, Samuel Greenbank, Guanchen Li, David A. Howey, Charles W. Monroe

andrew.wang@eng.ox.ac.uk (A.A.W.)
charles.monroe@eng.ox.ac.uk (C.W.M.)

## Highlights

Applied current rearranges neutral cosolvents in lithium-ion electrolytes

A solution-property machine-learning model pinpoints electrolyte composition changes

This polarization effect is expected to be most severe near electrode interfaces

Wang et al., Cell Reports Physical Science 3, 101047
September 21, 2022 
https://doi.org/10.1016/j.xcrp.2022.101047

Cell Reports
Physical Science

CellPress
OPEN ACCESS

Article

# Current-driven solvent segregation in lithium-ion electrolytes

Andrew A. Wang,[1,2,*] Samuel Greenbank,[1] Guanchen Li,[1,2,3] David A. Howey,[1,2] and Charles W. Monroe[1,2,4,*]

## SUMMARY

**Liquid lithium-battery electrolytes universally incorporate at least two solvents to balance conductivity and viscosity. Almost all continuum models treat cosolvent systems such as ethylene carbonate:ethyl-methyl carbonate (EC:EMC) as single entities whose constituents travel with identical velocities. We test this "single-solvent approximation" by subjecting $LiPF_6$:EC:EMC blends to constant-current polarization in Hittorf experiments. A Gaussian process regression model trained on physicochemical properties quantifies changes in composition across the Hittorf cell. EC and EMC are found to migrate at noticeably different rates under applied current, demonstrating conclusively that the single-solvent approximation is violated and that polarization of salt concentration is anticorrelated with that of EC. Simulations show extreme solvent segregation near electrode/liquid interfaces: a 5% change in EC:EMC ratio, post-Hittorf polarization, implies more than a 50% change adjacent to the interface during the current pulse. Understanding how lithium-ion flux induces local cosolvent or additive imbalances suggests new approaches to electrolyte design.**

## INTRODUCTION

Contemporary lithium-ion electrolytes are formulated as mixed-solvent systems, a paradigm that balances competing requirements including interfacial and chemical stability, high ionic conductivity, and low solution viscosity. Pioneering previous work showed that high-viscosity, high-permittivity ethylene carbonate (EC) could be combined with low-viscosity, low-permittivity linear carbonates to meet these criteria.[2,3] New cosolvent blends have been designed for advanced applications such as fast charging or compatibility with lithium-metal electrodes using analogous design targets. Recent research has focused on innovative concepts such as ultra-concentrated "solvent-in-salt" electrolytes[4] or "localized high-concentration" electrolytes, wherein high-molarity solvate structures are dispersed within a diluent cosolvent.[5] Developing quantitative understanding of how ions and cosolvents distribute and interact between electrodes is fundamentally important for the future design and optimization of electrochemical energy storage systems.

Preferential solvation[6] between cosolvents and lithium salts on microscopic length scales has been investigated with both spectroscopic experiments[7–9] and quantum-chemical simulations.[10,11] Recently, von Wald Cresce and colleagues reported that lithium hexafluorophosphate ($LiPF_6$) in a bulk 3:7 mol-ratio mix of EC and ethyl-methyl carbonate (EMC) had a 7:3 EC:EMC coordinated-solvent population ratio within the $Li^+$ solvation shell.[7] This competitive-solvation phenomenon is

[1]Department of Engineering Science, University of Oxford, Oxford OX1 3PJ, UK

[2]The Faraday Institution, Didcot OX11 0RA, UK

[3]James Watt School of Engineering, University of Glasgow, Glasgow G12 8QQ, UK

[4]Lead contact

*Correspondence: andrew.wang@eng.ox.ac.uk (A.A.W.), charles.monroe@eng.ox.ac.uk (C.W.M.)

https://doi.org/10.1016/j.xcrp.2022.101047

understood to correlate with solid-electrolyte interphase (SEI) formation and degradation side reactions in lithium-ion batteries.[12] Beyond microscopic studies, recent work by Miele et al. used Raman optical fibers to reveal local swings in solvation dynamics and EC:EMC ratio within full Li-ion cells during operation.[13] Additional spatial resolution is needed to determine how these changes vary across the domain between electrodes.

At the continuum level, mass transport and thermodynamics in binary electrolytes has been resolved with remarkable fidelity. For a binary system comprising a single solvent and a lithium salt, a consistently parameterized transport model based on Newman's concentrated-solution theory[14,15] can very accurately predict spatiotemporal ion distributions under dynamic polarization conditions.[16,17] The solvent is also increasingly being recognized as a mobile component in and of itself.[18–20] Various groups have measured bulk velocities of both polymer and liquid electrolytes directly, demonstrating that solvents can migrate under applied currents, despite being charge-neutral chemical species.[17,21,22]

Given the confirmed presence of solvent drift on the macroscale and preferential ion solvation on the microscale, a question arises: do the different cosolvent species in lithium electrolytes move together? This query was aptly raised in a recent communication by Mistry and Srinivasan.[23] Previous transport characterizations of mixed-solvent lithium-ion battery electrolytes have universally applied a pseudo-single-solvent approximation, whereby cosolvents are treated as a single entity,[24–26] which presumes that each species making up the solvent blend moves at the same rate. Note that this approximation is born out of prohibitive experimental complexity rather than decisive experimental justification—even a simple cosolvent electrolyte such as $LiPF_6$:EC:EMC, made up of two solvents and a simple salt, requires the parametrization of six independent transport coefficients and six thermodynamic parameters to describe isothermal, isobaric, locally electroneutral transport.[14] If cosolvent motion is not perfectly correlated at the continuum scale, then the differences in transport rates among solvents could be exploited, both to fine-grain electrolyte simulations and to develop new routes for electrolyte design and discovery.

A rigorous test of the single-solvent approximation must probe whether applied current or salt-concentration polarization induces segregation of cosolvent species. To that end, we performed Hittorf experiments (Figure 1A) to induce salt-composition differences across solutions of $LiPF_6$ salt in a 1:1 mass ratio of EC:EMC cosolvent and investigated whether and how polarization of the salt concentration correlates with polarization of the solvent ratio. This application of a Hittorf cell requires accurate estimation of ternary electrolyte composition, which cannot be achieved with the purely gravimetric or conductometric strategies used in the past.[15,27] Chemical compositions of the $LiPF_6$:EC:EMC solutions extracted from Hittorf cells were therefore determined using a machine-learning approach, based on a Gaussian process regression model trained with a database of precise physicochemical property data. Alternative approaches to composition measurements based on spectroscopy are a poor fit for this problem, both because of the expected low magnitude of solvent polarization and the chemical similarity of the EC and EMC molecules. Below, we report a significant degree of current-driven solvent segregation during Hittorf experiments, showing that $LiPF_6$:EC:EMC indeed violates the single-solvent approximation.

To understand the impact of solvent segregation more clearly, we implement a four-species multicomponent transport model based on Onsager-Stefan-Maxwell theory

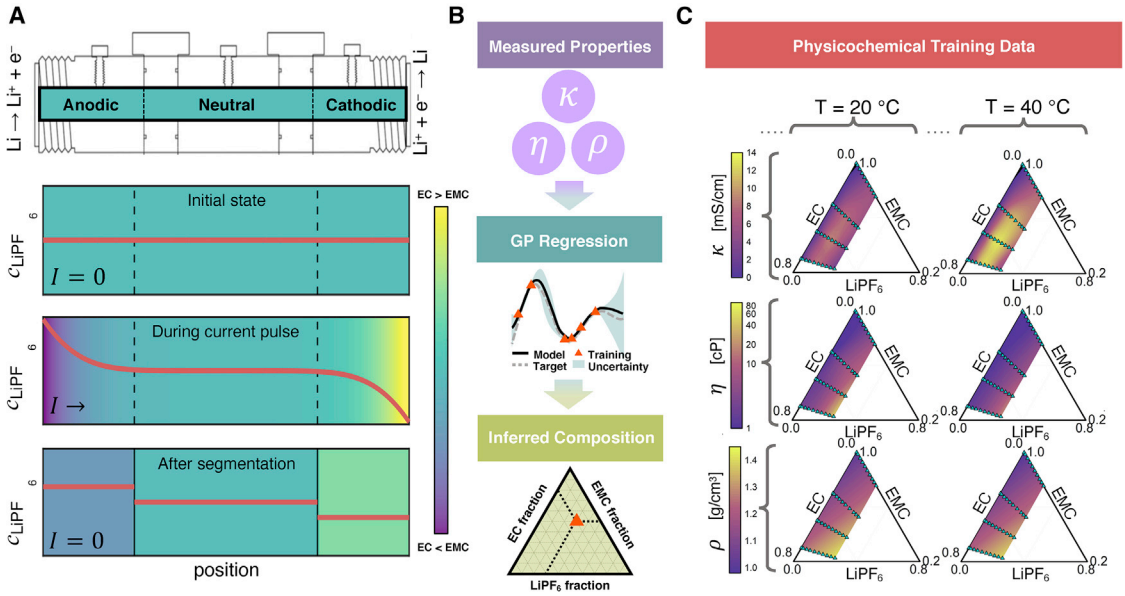


**Figure 1. Hittorf experiment and Gaussian process regression analysis of cosolvent segregation**

(A) Hittorf cell schematic, showing the valved anodic, neutral, and cathodic chambers in the symmetric cylindrical Li|electrolyte|Li cell. Initially, (top) the electrolyte has uniform distributions of salt concentration (red curve) and solvent ratio (background color). As current is passed through the cell (middle), it induces both salt and cosolvent gradients. The valves are then sealed, and each chamber equilibrated (bottom), yielding solutions that are extracted to determine the volume-averaged changes of salt and solvent content in the anodic and cathodic chambers.

(B) Conductivity, viscosity, and density measurements are made at 10°C, 20°C, 25°C, 30°C, and 40°C for the electrolytes extracted from the Hittorf cell's anodic and cathodic chambers. A Gaussian process regression model, trained on the dataset of known solvent compositions illustrated in (C), is then used to infer the $LiPF_6$, EC, and EMC mass fractions of the electrolytes extracted from the Hittorf cell.

(C) Physicochemical training datasets for the Gaussian process regression model. Ternary diagrams show the solution conductivity κ, viscosity η, and density ρ (values indicated by scale bars) for $LiPF_6$:EC:EMC electrolytes from 0 to 2 M with EC:EMC mass ratios of 0:1, 3:7, 1:1, and 7:3 (the measured mass fractions are shown as points on the ternary diagrams) at 20°C and 40°C. The rest of the training data, at additional temperatures of 10°C, 25°C, and 30°C, are plotted in Figure S2.

to estimate what the Hittorf experiment results—which average current-induced concentration polarization over large volumes—imply about the local cosolvent composition. The transport model suggests that cosolvent ratios change dramatically near electrode surfaces, a local effect that could be tracked to refine degradation or SEI-formation models based on reactions involving EC. Cosolvation environments in liquid electrolytes can also impact the energetics and dynamics of fundamental electrochemical processes relevant to lithium-ion batteries, such as intercalation, electrodeposition, and side reactions.

## RESULTS AND DISCUSSION

### Data-driven composition analysis

Hittorf experiments were performed using the methodology shown schematically in Figure 1A. (More details are provided in the experimental procedures.) Note that the gravimetric Hittorf approach implemented by Hou and Monroe relies on the direct dependence of density on solute concentration in an isothermal binary solution[15,28] and is inadequate for applications to cosolvent electrolytes. For example, raising the molarity of either $LiPF_6$ or EC in a $LiPF_6$:EC:EMC ternary will increase the solution's density. Hittorf experiments also require sensitivity to very small concentration changes because species molarity changes induced by the applied current pulse are diluted across the entire volume of each Hittorf-cell chamber before its composition assay.[29] Hence, quantitative analytical methods such as confocal Raman spectroscopy, which require careful deconvolution of peak signals, were deemed to have

resolution too low for this study. Instead, the Gaussian process (GP) model illustrated in Figure 1B and trained on the datasets from Figure 1C was used to infer the extent of solvent polarization induced by a current pulse in a Hittorf cell.

The GP model learned from electrolyte properties is found to predict ternary solution compositions with very high precision. This owes in part to the widely differing trends in how density, viscosity, and ionic conductivity of $LiPF_6$:EC:EMC solutions vary with respect to composition and temperature. Density follows a relatively linear functionality with respect to species molarity, whereas viscosity can vary exponentially; conductivity passes through local maxima with respect to both the salt and EC contents.[30,31] Importantly, all three physicochemical properties can be measured to several digits of precision under temperature-controlled conditions using standard commercial equipment. Figures 1C and S2 show solution density, viscosity, and ionic conductivity from 0 to 2 M $LiPF_6$ concentration in solutions with EC:EMC mass ratios of 0:1, 3:7, 1:1, and 7:3 at temperatures of 10°C, 20°C, 25°C, 30°C, and 40°C. These measurements provide a comprehensive set of input data for a regression model whose output is ternary composition of the electrolyte. Property measurements at varying cosolvent and salt fractions, plotted in Figure 1C, were used to train the GP regression model for composition assay. The average root-mean-square error for mass fractions calculated from leave-one-out cross-validation was found to be $0.003 \pm 0.002$ when predicting the salt and EMC composition, corresponding to uncertainties of approximately 2.4% and 0.7% for the $LiPF_6$ and EMC mass fractions, respectively (Note S1; Figures S3 and S4).

It is notable that the present application of machine-learning methods aims to predict an electrolyte's composition given its properties, whereas almost all computational-materials work to date has aimed to address the inverse problem, i.e., prediction or optimization of properties given composition.[32,33] GP regression is a flexible non-parametric method that makes few assumptions about data-fitting functionality. It is also a Bayesian approach that inherently estimates the uncertainty of predictions.[34] All the physicochemical property data, as well as an implementation of the GP model in the GPy Python framework,[35] are provided in the supplemental experimental procedures, Figure S1, and data repository that accompany this article.[1]

### Hittorf results indicate cosolvent segregation

A series of 1:1 mass ratio EC:EMC electrolytes with salt mass fractions of 0.065, 0.125, and 0.185 (approx. 0.6, 1.0, and 1.6 M, respectively) were polarized within Hittorf cells under an applied current of 0.5 mA (0.64 $mAcm^{-2}$) for 20 h. Buoyancy effects were suppressed by orienting the long axis of the Hittorf cells vertically and choosing the sign of current to ensure that plating occurred on the top electrode. Immediately following the passage of charge, the valves separating the anodic, neutral, and cathodic chambers were sealed, and the solutions in the individual chambers were mixed with stir bars to homogenize their compositions before density, conductivity, and viscosity were measured at the five temperatures mentioned previously. The GP model was then used to map the resultant set of property measurements into $LiPF_6$, EC, and EMC mass fractions based on both the magnitudes of the three properties and their relative trends across the five temperatures.

Solvent segregation is clearly observed, indicating that EC and EMC do not move as a single entity. Figure 2 presents a ternary diagram showing the results of Hittorf polarization tests for electrolytes with three different concentrations of $LiPF_6$. All three

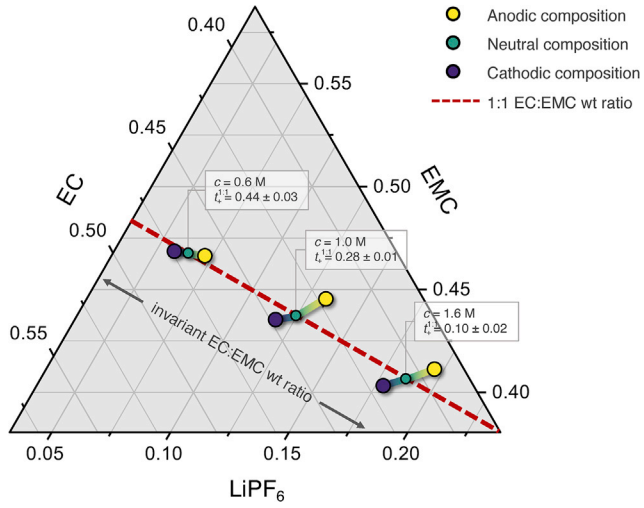


**Figure 2. Comparison of Hittorf polarizations with predictions of the single-solvent approximation**

Ternary diagram showing anodic- (yellow), neutral- (green), and cathodic-chamber (blue) mass fractions of EC, EMC, and $LiPF_6$ after Hittorf experiments for three salt molarities (0.6, 1.0, 1.6 M) in a 1:1 (by mass) EC:EMC solvent. The marker size encompasses error, accounting both for experimental repeats and variance in the GP prediction, as discussed in Note S1. The red dashed line indicates an invariant EC:EMC ratio. Since the dumbbell markers for each Hittorf result are not parallel to this line, the single-solvent approximation is not upheld.

initial compositions (green markers) begin with the same 1:1 cosolvent mass ratio, and as such, they lie along the dashed red curve on the figure. For each of the polarized solutions, the salt concentration is elevated in the anodic chamber (yellow markers) and depleted in the cathodic chamber (purple markers). If EC and EMC were to migrate with identical velocities, then the anodic and cathodic compositions would be polarized along the line of invariant solvent ratio (red dashed line). This is not the case, however, demonstrating that the single-solvent approximation does not hold. Despite the Hittorf experiment operating above the limiting current density in a semi-infinite geometry, we discuss later and show in Figure 4B that considerable solvent segregation is still expected across geometries relevant to practical Li-ion cells cycling below the limiting current.

The extent of current-driven solvent segregation also increases as salt content rises, indicating that the solvent mobilities are sensitive to ion molarity. For the 1.0 M salt concentration, the final EC:EMC ratios were 0.96:1 and 1.03:1 in the anodic and cathodic Hittorf chambers, respectively, resulting in an EC mass-fraction difference of 5.1% across the cell. (It should be emphasized that this is the concentration difference that remains after the concentration profiles in surface boundary layers are averaged across the entire chambers of the Hittorf cell.) Full experimental data are provided in the data repository associated with this article.

Notably, the EMC composition ratio was observed to increase in the anodic chamber, indicating a propensity for EMC, rather than EC, to move with $LiPF_6$. This contrasts the results of equilibrium solvation studies, which generally conclude that EC is more tightly bound to the $LiPF_6$ salt.[7] The counterintuitive result that EC moves against the salt gradient suggests that a dynamical drag interaction—independent of the classically expected solvation interaction based on the dielectric constant of the solvent species—may be inducing solvent segregation under applied current.

This observation can also be considered in light of the coordination numbers reported for cyclic and linear carbonates.[9–11] By assuming a solvated mobile cation with the structure $[Li(EC)_3(EMC)]^+$, and with the uncoordinated EC and EMC treated with a single-solvent approximation, one would expect that Hittorf polarization of 1 M $LiPF_6$ in a 1:1 mass ratio of EC:EMC (6.2 M of EC and 5.3 M of EMC) would result in final EC:EMC ratios of 1.04:1 and 0.98:1 in the anodic and cathodic Hittorf chambers, respectively—almost exactly opposed to the result reported here.

We expect the solvent-segregation effect quantified here to impact transport-property characterization for practical lithium electrolytes. Effective cation transference numbers $t_+^{1:1}$ were determined using the $Li^+$ composition changes estimated by GP regression, under an assumption that the cosolvent retains the partial molar volume of neat 1:1 EC:EMC as it is polarized. (Details are provided in Note S4.) The $t_+^{1:1}$ value was found to decrease from 0.44 to 0.10 as the salt concentration rose from 0.6 to 1.6 M, following a trend consistent with results from similar studies of $LiPF_6$ electrolytes in solvent mixtures made up of cyclic and linear carbonates.[24,26] If galvanostatic and potentiostatic methods induce salt polarization along with a cosolvent-ratio gradient, the degree of cosolvent segregation will vary with experimental conditions and may be a factor contributing to the wide spread of reported transport-property measurements in the literature, such as those discussed by Bergstrom et al.[25] Extending potentiometric magnetic resonance imaging (MRI) studies to capture dynamic solvent profiles would provide a path to parameterize these electrolyte systems more rigorously within the concentrated-solution-theory framework.[16]

## Amplification of polarization at boundaries

Hittorf-cell results only reveal a volume-averaged change in electrolyte composition after polarization. It is expected that current-induced polarization of both salt concentration and solvent ratio should be focused within boundary layers near the electrolytes' interfaces, as shown schematically in Figure 1A. The transient degree of local solvent segregation may be estimated quantitatively using a four-species multicomponent transport model for the $LiPF_6$:EC:EMC system. Adopting the system of Onsager-Stefan-Maxwell equations presented earlier by Monroe,[36] originally derived for metal/oxygen batteries with a binary electrolyte and an additional dissolved neutral species, the cation flux $\vec{N}_+$ and EC flux $\vec{N}_o$ can be expressed as

$$\vec{N}_+ = -D_e\vec{\nabla}c - D_\times\left\langle\frac{c}{c_T}\right\rangle\vec{\nabla}c_o + t_+^0\frac{\vec{i}}{F} \quad (1)$$

$$\vec{N}_o = -D_\times\left\langle\frac{c_o}{c_T}\right\rangle\vec{\nabla}c - D_o\vec{\nabla}c_o - \Xi\frac{\vec{i}}{F} \quad (2)$$

if convection is neglected. Here, $F$ is Faraday's constant; $c$, $c_o$, and $c_T$ are the $LiPF_6$, EC, and total solution concentrations, respectively; $D_e$ and $D_o$ are, respectively, the Fickian diffusion coefficients of salt and EC in EMC; and $D_\times$ is the cross-diffusivity, which describes how one solute gradient induces flux of the other solute. The cation transference number $t_+^0$ and EC electro-osmotic coefficient $\Xi$ describe how $Li^+$ and EC, respectively, migrate through EMC in response to an applied current density $\vec{i}$. Material balances and boundary conditions that close these flux laws are detailed in Note S1. Although Equations 1 and 2 neglect convection, it could be included following the method of Liu and Monroe.[18]

Solvent segregation effects can be extreme near interfaces. In a Hittorf measurement of $LiPF_6$:EC:EMC that yields a $\pm$5% swing in the volume-averaged EC:EMC

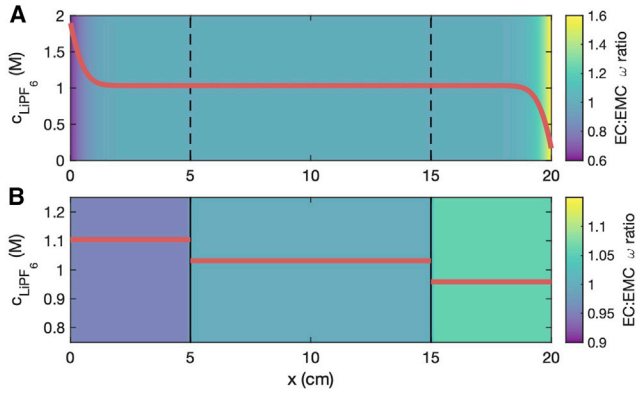


**Figure 3. Dynamic Hittorf salt and solvent compositions predicted by four-component transport model**

(A) Simulated maximum degree of polarization of the 1 M $LiPF_6$ in 1:1 mass ratio EC:EMC electrolyte before current cutoff during a Hittorf experiment. Salt concentration is shown with red curves, while solvent ratio is represented by the background colormap. Based on parameter estimates, model simulations show that the majority of solvent segregation occurs in boundary layers very close to the electrode surfaces.

(B) Electrolyte compositions after both Hittorf valves (locations shown by solid vertical lines) are sealed off and the salt and solvent gradients in (A) are allowed to come to equilibrium in each chamber. It is these final compositions that are inferred from property measurements using the GP regression model.

ratio, such as the data points measured in the ternary plot Figure 2, the electrode surfaces experience more than $\pm$50% excess EC interfacial content during a current pulse. This result is found by solving a transport problem governed by Equations 1 and 2, which allows one to simulate the degree of solvent polarization near the electrode interfaces that is commensurate with the solution concentrations extracted from the Hittorf cell chambers. As a first approximation, transport parameters were assumed to be composition independent. We took $D_e = 3 \times 10^{-10}$ $m^2s^{-1}$, a value measured for the $LiPF_6$:EMC binary,[16] and $D_o = 5 \times 10^{-10}$ $m^2s^{-1}$, as observed by pulsed-gradient spin-echo nuclear magnetic resonance (NMR).[9] The cation transference number was set at $t_+^0 = 0.24$, as measured here using the standard Hittorf equation. Like the transference number, the electro-osmotic coefficient $\Xi$ can also be extracted from the Hittorf experiment using the change in EC compositions estimated by the GP model. From the GP inferences of net moles of EC moved to the anodic Hittorf chamber, one finds that $\Xi \approx -1.4 \pm 0.1$. Since a precise value of cross-diffusivity is not known, we assumed that $D_x = 0$, a value that should provide a lower bound on the change in the interfacial solvent ratio. Figures 3A and 3B compare the maximum degree of polarization during the 1.0 M Hittorf experiment with the equilibrated results using the above parameters. With higher values of cross-diffusivity $D_x$, the solvent swing at the interfaces would be even more severe.

To inform general expectations about current-induced cosolvent segregation in practical lithium-ion-battery electrode geometries, it is useful to observe composition gradients under an applied limiting current density for the 1.0 M $LiPF_6$ EC:EMC 1:1 mass ratio electrolyte. The limiting current density is the largest steady-state current that can be imposed before the charge-carrying salt is completely depleted at the cathode. At the limiting current, gradients of both salt and solvent concentration are sustained across the entire interelectrode gap, as can be seen from the plot of normalized steady-state molarity with respect to dimensionless position across the gap in Figure 4B. Figure 4A presents a contour plot expressing the sensitivity of the EC:EMC mass ratio to the cross diffusivity $D_x$ and EC

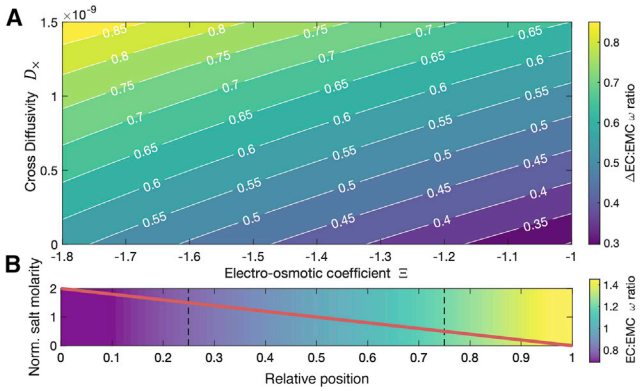


**Figure 4. Generalized degree of solvent-segregation under steady limiting-current conditions**

(A) Sensitivity sweep of the absolute change in interfacial EC:EMC mass ratio, shown as a contour plot with respect to the cross-diffusivity and electro-osmotic coefficient (two transport properties unique to the four-species electrolyte model), for an electrolyte polarized under limiting-current conditions. For example, the 0.45 ΔEC:EMC contour refers to an average polarized electrode boundary EC:EMC solvent ratio of 1.45:1 and 1:1.45 from the initial neutral composition of 1:1 mass ratio EC:EMC with 1 M $LiPF_6$.

(B) Limiting current salt red curve) and solvent-ratio profile (background colormap) for the same initial solvent ratio, with a normalized salt composition and inter-electrode distance.

electro-osmotic coefficient Ξ. The range studied for $D_x$ represents the bounds based on thermodynamic stability that $0 \leq D_x < D_e c_T / 2c$.[36] Each colored band represents the possible change—both increase and decrease—in the EC:EMC mass ratio on either boundary of the electrolyte. For example, the 0.45 contour represents the set of parameters that could segregate an initial 1:1 EC:EMC bulk solution to a 1.45:1 and 1:1.45 ratio at the cathode and anode, respectively.

Cosolvent composition variation also alters the electrochemical properties of the electrolyte with respect to its position between the electrodes. For example, (de)solvation energies and kinetics of electrochemical reactions are impacted by the solvation environment of $Li^+$. Similarly, the electrolyte composition immediately adjacent to the electrode surface will directly alter the nature of SEI formation reactions and SEI composition itself. Continuum-level modelling has shown that electrolyte transport and thermodynamic properties that vary as functions of both salt molarity and temperature are necessary to predict battery behavior during operational extremes.[26] The results reported here suggest that such higher-fidelity simulations may need to be broadened to include changes in solvent ratios as well. Significantly, in the case of the anodic interface in Figure 4B, the predicted viscosity varies by 22%, based on whether cosolvent segregation is accounted for or not.

It has been demonstrated that, contrary to the conventional assumption, cosolvents in lithium-ion electrolytes do not move together in fixed proportion when facilitating charge transport. The reported test of the single-solvent approximation relied on a combination of Hittorf experiments and a GP regression model, trained with a database of physicochemical electrolyte properties, which was used to infer composition from property measurements. A four-species multicomponent transport simulation was then used to estimate the degree of cosolvent polarization at interfaces. This solvent-segregation phenomenon could be studied with finer spatial resolution using *in situ* techniques such as potentiometric MRI or chemical shift imaging. Spatiotemporal measurements of specific solvents under dynamic cycling will enable further understanding of counterintuitive observations such as why EMC, rather than EC, migrates preferentially alongside $Li^+$. The results emphasize that solvent

compositions in batteries not only vary gradually over cycle life, due to decomposition-reaction consumption, but can also experience local intra-cycle variation, induced by current flow. The balance between the two should be studied in practical cell geometries. Cosolvent segregation is expected to occur in any situation where Faradaic electrode reactions (intercalation or conversion/plating) induce salt gradients. Our findings suggest that future experiments to track solvent concentrations would enable the parametrization of advanced physics-based models that include local interfacial EC content, which could elucidate more accurate kinetic models of interfacial reactions such as Li intercalation, Li plating, and SEI formation. Key physical insights in this work show that macroscopic states should also be considered alongside microscopic solvation environments when determining electrolyte behavior. The same framework used to describe the $LiPF_6$:EC:EMC electrolyte here can also be applied to novel formulations and solution additives to aid the simulation, design, and discovery of higher-performing next-generation batteries.

## EXPERIMENTAL PROCEDURES

### Resource availability

#### *Lead contact*

Further information and requests for resources and reagents should be directed to and will be fulfilled by the lead contact, Charles W. Monroe (charles.monroe@eng.ox.ac.uk).

#### *Materials availability*

This study did not generate new unique materials.

#### *Data and code availability*

The datasets generated during this study are available on GitHub:[1] https://doi.org/10.5281/zenodo.6299956.

### Electrolyte formulation and physicochemical property measurements

Density, viscosity, and conductivity measurements were performed on both electrolytes extracted from Hittorf polarization cells and the standard solutions used to train the property-composition GP regression model. Initial solutions were prepared within an argon glovebox (Inert Technologies) with vacuum-dried $LiPF_6$ (99.99%, battery grade, Sigma Aldrich) and EC (99%, Sigma Aldrich) and EMC (99.9%, Sigma Aldrich) solvents that were stored under 3 Å molecular sieves. Pure EC was first melted, and solutions were formulated based on mass fractions using an analytical balance (OHAUS). Densities and dynamic viscosities were measured inside the glovebox with a high-precision oscillating densitometer with in-line rolling-ball viscometer attachment (DMA4100, Anton Paar). Ionic conductivities were measured with an AC conductivity probe (Orion A212, Thermo Fisher Scientific) in a sealed cell with a temperature-controlled water bath (Arctic A25, Thermo Fisher Scientific). Measurements were taken at increasing temperatures of 10°C, 20°C, 25°C, 30°C, and 40°C.

### Hittorf cell experimental procedure

The Hittorf cell (Figure 1A) is a long cylindrical symmetric Li-Li polarization cell. The central cavity has two configurations, open and closed, where two stopcocks can be sealed to separate the cylinder into anodic, neutral, and cathodic chambers. Lithium electrodes on either end of the Hittorf cell were prepared by polishing Li foil (99.9% Alfa Aesar) with a PTFE brush before punching it into discs. Electrolyte was loaded into the Hittorf cell under the open configuration. The cell was sealed and oriented vertically. A constant current of 0.5 mA was applied for 20 h (PGSTAT302N, Metrohm) to induce salt and solvent concentration gradients in the anodic and cathodic

chambers. Immediately after the current was interrupted, the cell was set in the closed configuration. After each individual chamber's composition had equilibrated (1 h of stirring with a magnetic stir bar), the electrolytes were extracted, and their physicochemical properties were measured. More detailed information, including a theoretical analysis of the Hittorf experiment for a binary electrolyte, were discussed by Hou et al.[14] and Wang et al.[15,28]

### GP regression model

The GP model was implemented in the GPy Python framework,[35] with a squared-exponential radial basis function (RBF) kernel and an automatic relevance determination (ARD) structure. The model was trained on input data consisting of solution density, viscosity, and conductivity at 10°C, 20°C, 25°C, 30°C, and 40°C. Each set of 15 input data points is linked through the GPR model to a single set of composition outputs, the mass fractions of $LiPF_6$ and EMC, with that of EC being inferred by subtraction of the other two fractions from unity. Cross-validation using the leave-one-out method was performed on the GPR model. The average root-mean-square error for mass fractions was found to be $0.003 \pm 0.002$, corresponding to an uncertainty of approximately 2.4% and 0.7% for $LiPF_6$ and EMC mass fractions, respectively. The code and data used for the GPR model is accessible at the accompanying data repository.[1]

## SUPPLEMENTAL INFORMATION

Supplemental information can be found online at https://doi.org/10.1016/j.xcrp.2022.101047.

## ACKNOWLEDGMENTS

This work was supported by the Faraday Institution Multiscale Modelling Project, subaward FIRG025 under EPSRC grant number EP/S003053/1.

## AUTHOR CONTRIBUTIONS

Conceptualization, A.A.W., G.L., and C.W.M.; methodology, A.A.W., S.G., and C.W.M.; investigation, A.A.W.; formal analysis, A.A.W. and S.G.; writing – original draft, A.A.W.; writing – review & editing, D.A.H. and C.W.M.; supervision, D.A.H. and C.W.M.

## DECLARATION OF INTERESTS

The authors declare no competing interests.

Received: March 22, 2022
Revised: July 1, 2022
Accepted: August 22, 2022
Published: September 8, 2022

## REFERENCES

1. Wang, A.A. (2022). Data and code repository. Preprint at Zenodo. https://doi.org/10.5281/zenodo.6299956.
2. Xu, K. (2004). Nonaqueous liquid electrolytes for lithium-based rechargeable batteries. Chem. Rev. *104*, 4303–4417.
3. Hall, D.S., Self, J., and Dahn, J.R. (2015). Dielectric constants for quantum chemistry and Li-ion batteries: solvent blends of ethylene carbonate and ethyl methyl carbonate. J. Phys. Chem. C *119*, 22322–22330.
4. Borodin, O., Self, J., Persson, K.A., Wang, C., and Xu, K. (2020). Uncharted waters: super-concentrated electrolytes. Joule *4*, 69–100.
5. Cao, X., Jia, H., Xu, W., and Zhang, J.-G. (2021). Review—localized high-concentration electrolytes for lithium batteries. J. Electrochem. Soc. *168*, 010522.
6. Feakins, D., O'Neill, R., and Waghorne, E. (1982). Preferential solvation of ions and solvent transport. Pure Appl. Chem. *54*, 2317–2326.
7. Von Wald Cresce, A., Borodin, O., and Xu, K. (2012). Correlating Li+ solvation sheath structure with interphasial chemistry on graphite. J. Phys. Chem. C *116*, 26111–26117.
8. Bogle, X., Vazquez, R., Greenbaum, S., Cresce, A.V.W., and Xu, K. (2013).

Understanding Li+-solvent interaction in nonaqueous carbonate electrolytes with 17O NMR. J. Phys. Chem. Lett. *4*, 1664–1668.

9. Uchida, S., and Kiyobayashi, T. (2021). How does the solvent composition influence the transport properties of electrolyte solutions? LiPF6 and LiFSA in EC and DMC binary solvent. Phys. Chem. Chem. Phys. *23*, 10875–10887.

10. Borodin, O., Olguin, M., Ganesh, P., Kent, P.R.C., Allen, J.L., and Henderson, W.A. (2016). Competitive lithium solvation of linear and cyclic carbonates from quantum chemistry. Phys. Chem. Chem. Phys. *18*, 164–175.

11. Seo, D.M., Reininger, S., Kutcher, M., Redmond, K., Euler, W.B., and Lucht, B.L. (2015). Role of mixed solvation and ion pairing in the solution structure of lithium ion battery electrolytes. J. Phys. Chem. C *119*, 14038–14046.

12. Xu, K., Lam, Y., Zhang, S.S., Jow, T.R., and Curtis, T.B. (2007). Solvation sheath of Li+ in nonaqueous electrolytes and its implication of graphite/electrolyte interface chemistry. J. Phys. Chem. C *111*, 7411–7421.

13. Miele, E., Dose, W.M., Manyakin, I., Frosz, M.H., Ruff, Z., De Volder, M.F.L., Grey, C.P., Baumberg, J.J., and Euser, T.G. (2022). Hollow-core optical fibre sensors for operando Raman spectroscopy investigation of Li-ion battery liquid electrolytes. Nat. Commun. *13*, 1651–1710.

14. Newman, J., and Thomas-Alyea, K.E. (2004). Electrochemical Systems 3, illustr ed. (John Wiley & Sons).

15. Hou, T., and Monroe, C.W. (2020). Composition-dependent thermodynamic and mass-transport characterization of lithium hexafluorophosphate in propylene carbonate. Electrochim. Acta *332*, 135085.

16. Wang, A.A., Gunnarsdóttir, A.B., Fawdon, J., Pasta, M., Grey, C.P., and Monroe, C.W. (2021). Potentiometric MRI of a superconcentrated lithium electrolyte: testing the irreversible thermodynamics approach. ACS Energy Lett. *6*, 3086–3095.

17. Steinrück, H.G., Takacs, C.J., Kim, H.K., MacKanic, D.G., Holladay, B., Cao, C., Narayanan, S., Dufresne, E.M., Chushkin, Y., Ruta, B., et al. (2020). Concentration and velocity profiles in a polymeric lithium-ion battery electrolyte. Energy Environ. Sci. *13*, 4312–4321.

18. Liu, J., and Monroe, C.W. (2014). Solute-volume effects in electrolyte transport. Electrochim. Acta *135*, 447–460.

19. Farkhondeh, M., Pritzker, M., Delacourt, C., Liu, S.S.W., and Fowler, M. (2017). Method of the four-electrode electrochemical cell for the characterization of concentrated binary electrolytes: theory and application. J. Phys. Chem. C *121*, 4112–4129.

20. Mistry, A., Grundy, L.S., Halat, D.M., Newman, J., Balsara, N.P., and Srinivasan, V. (2022). Effect of solvent motion on ion transport in electrolytes. J. Electrochem. Soc. *169*, 040524.

21. Schmidt, F., and Schönhoff, M. (2020). Solvate cation migration and ion correlations in solvate ionic liquids. J. Phys. Chem. B *124*, 1245–1252.

22. Halat, D.M., Fang, C., Hickson, D., Mistry, A., Reimer, J.A., Balsara, N.P., and Wang, R. (2022). Electric-field-induced spatially dynamic heterogeneity of solvent motion and cation transference in electrolytes. Phys. Rev. Lett. *128*, 198002.

23. Mistry, A., and Srinivasan, V. (2021). Do we need an accurate understanding of transport in electrolytes? Joule *5*, 2773–2776.

24. Valoen, L.O., and Reimers, J.N. (2005). Transport properties of LiPF6-based Li-ion battery electrolytes. J. Electrochem. Soc. *152*, A882.

25. Bergstrom, H.K., Fong, K.D., and Mccloskey, B.D. (2021). Interfacial effects on transport coefficient measurements in Li-ion battery electrolytes. J. Electrochem. Soc. *168*, 060543.

26. Landesfeind, J., and Gasteiger, H.A. (2019). Temperature and concentration dependence of the ionic transport properties of lithium-ion battery electrolytes. J. Electrochem. Soc. *166*, A3079–A3097.

27. Steel, B.J., and Stokes, R.H. (1958). A Hittorf transference number apparatus employing conductimetric analysis of the solutions. J. Phys. Chem. A *62*, 450–452.

28. Wang, A.A., Hou, T., Karanjavala, M., and Monroe, C.W. (2020). Shifting-reference concentration cells to refine composition-dependent transport characterization of binary lithium-ion electrolytes. Electrochim. Acta *358*, 136688.

29. Miele, E., Dose, W., Manyakin, I., Frosz, M., Grey, C., and Baumberg, J. (2021). Operando Raman Analysis of Electrolyte Changes in Li-Ion Batteries with Hollow-Core Optical Bre Sensors.

30. Ding, M.S., Xu, K., Zhang, S.S., Amine, K., Henriksen, G.L., and Jow, T.R. (2001). Change of conductivity with salt content, solvent composition, and temperature for electrolytes of LiPF[sub 6] in ethylene carbonate-ethyl methyl carbonate. J. Electrochem. Soc. *148*, A1196.

31. Logan, E.R., Tonita, E.M., Gering, K.L., Li, J., Ma, X., Beaulieu, L.Y., and Dahn, J.R. (2018). A study of the physical properties of Li-ion battery electrolytes containing esters. J. Electrochem. Soc. *165*, A21–A30.

32. Deringer, V.L., Bartók, A.P., Bernstein, N., Wilkins, D.M., Ceriotti, M., and Csányi, G. (2021). Gaussian process regression for materials and molecules. Chem. Rev. *121*, 10073–10141.

33. Dave, A., Mitchell, J., Kandasamy, K., Wang, H., Burke, S., Paria, B., Póczos, B., Whitacre, J., and Viswanathan, V. (2020). Autonomous discovery of battery electrolytes with robotic experimentation and machine learning. Cell Rep. Phys. Sci. *1*, 100264.

34. Rasmussen, C.E., and Williams, C.K.I. (2006). Gaussian Processes for Machine Learning (The MIT Press).

35. GPy (2012). GPy: a Gaussian process framework in python. http://github.com/SheffieldML/GPy.

36. Monroe, C.W. (2017). Does oxygen transport affect the cell voltages of metal/air batteries? J. Electrochem. Soc. *164*, E3547–E3551.